Diffusion of sodium ions in amorphous $Na_2Si_2O_5$: Quasielastic neutron scattering and *ab initio* molecular dynamics simulations

Mayanak K. Gupta, Sanjay K. Mishra, Ranjan Mittal, Baltej Singh, Prabhatasree Goel, Sanghamitra Mukhopadhyay, Rakesh Shukla, Srungarpu N. Achary, Avesh K. Tyagi, and Samrath L. Chaplot

Published version information

Citation: MK Gupta et al. "Diffusion of sodium ions in amorphous $Na_2Si_2O_5$: Quasielastic neutron scattering and *ab initio* molecular dynamics simulations." Physical Review Materials, vol. 4, no. 4 (2020): 045802.

DOI: 10.1103/PhysRevMaterials.4.045802

Diffusion of sodium ions in amorphous $Na_2Si_2O_5$: Quasielastic neutron scattering and *ab initio* molecular dynamics simulations

Mayanak K. Gupta,[1,*] Sanjay K. Mishra,[1] Ranjan Mittal,[1,2,†] Baltej Singh,[1,2] Prabhatasree Goel,[1] Sanghamitra Mukhopadhyay,[4] Rakesh Shukla,[3] Srungarpu N. Achary,[2,3] Avesh K. Tyagi,[2,3] and Samrath L. Chaplot[1,2]

[1]*Solid State Physics Division, Bhabha Atomic Research Centre, Mumbai 400085, India*

[2]*Homi Bhabha National Institute, Anushaktinagar, Mumbai 400094, India*

[3]*Chemistry Division, Bhabha Atomic Research Centre, Mumbai 400085, India*

[4]*ISIS Neutron and Muon Facility, Rutherford Appleton Laboratory, Chilton, Didcot, Oxon OX11 0QX, United Kingdom*

(Received 30 September 2019; revised manuscript received 12 March 2020; accepted 16 March 2020; published 8 April 2020)

The dynamics of Na ions in amorphous $Na_2Si_2O_5$, a potential solid electrolyte material for Na battery, have been investigated by employing. the quasielastic neutron scattering (QENS) technique in the temperature range 300 to 748 K. To understand the diffusion pathways and relaxation timescales of Na ionic diffusion, the experimental studies are complemented by *ab initio* and force-field molecular dynamics simulations. The QENS data are fairly well described by a jump-diffusion model with a mean jump length of about 3 Å and residence time about 9 ps. Our molecular dynamics simulations have predicted that the diffusion of Na^+ ions occurs in the amorphous phase of $Na_2Si_2O_5$ while absent in the crystalline orthorhombic phase even up to 1100 K. The molecular dynamics simulations have revealed that in the amorphous phase, due to different orientations of silicon polyhedral units, several accessible pathways are opened up for Na^+ diffusions. These pathways are not available in the crystalline phase of $Na_2Si_2O_5$ due to rigid spatial arrangement of silicon polyhedral units.

DOI: 10.1103/PhysRevMaterials.4.045802

I. INTRODUCTION

Clean and green storage of energy is achievable by various energy storage technologies [1–4]. Batteries are one of the most eligible devices [5–8] for this purpose. The solid-state batteries [6,9–13] offer a most compact and safe version to store energy at various scales. These batteries contain a solid electrolyte between two electrode materials and hence no separator is required to fabricate such batteries. The solid electrolyte [14], being more stable [6,9–11] than liquids, could resolve the issues of leakage, chemical stability, vaporization, flammability, and dendrites formation to a great extent. Also, they enable the use of metallic Li or Na as anode material [9,15] and enhanced current charge capacities.

A common feature to the most solid electrolyte materials is availability of sufficient number of atomic sites for the diffusing ions in the solid [16,17]. The diffusion process in the materials could be attributed to hopping of diffusing ions over these sites. There is no unique diffusion mechanism for all materials and a variety of diffusion mechanisms have been discovered in different materials based on their structural framework and nature of diffusing ions [17–20].

In search of an efficient and cost-effective Na and Li ion conductors for solid-state Na or Li-ion batteries there have been significant experimental and theoretical studies available in literature [21–28]. The diffusion of Li ions in these has been addressed by several experimental and theoretical modes, like tracer migration, positional displacement, as well as electrical property measurements. The positional displacement and site disorder of mobile ions often causes liquidlike sublattice in the frame of the rigid lattice. The crystalline $LiAlSiO_4$ (β-eucryptite) and Li_2X (X = O, S, Se) are known to exhibit Li-ion conductivity in the temperature range from 800 to 1400 K [25,29,30]. The inelastic neutron-scattering spectra of β-eucryptite at high temperature show significant broadening in the spectral regimes which is contributed by Li atoms [30]. The Li diffusion in β-eucryptite arises from highly correlated one-dimensional motion of Li channels along the hexagonal c axis [29]. The glass ceramics and amorphous solids like $Li_{3+x}PO_{4-x}N_x$(LiPON), A_7P_3S11(A = Li, Na), $A_{3-x}H_xOCl$ (A = Li, Na and $0 < x < 1$) and $Li_2S - P_2S_5$ have recently attracted attention [23,31–35] due to their much higher ionic conductivities at room temperature than their equivalent crystalline forms. The higher ionic conduction in amorphous phase than that in the crystalline phase might be due to creation of a significant number of percolative pathways with minimal energy barriers for ion migration, which is essentially a geometrical effect due to amorphization that promotes the ionic conduction. In the present case, the crystalline lattice has very little diffusion and amorphization provides essential pathways of diffusion. In other cases, where the crystal lattice strongly supports diffusion, amorphization might hinder some of the pathways and thereby reduce the diffusion.

Following the discovery of superionic Na-ion conduction in layered β-alumina, many Na-ion conductors have been discovered [36–40]. $Na_2Si_2O_5$ is known to show Na-ion conduction in its amorphous phase with ionic conductivity of 0.01 S/cm^2 at 500 °C [41]. At ambient pressure, $Na_2Si_2O_5$

*mayankg@barc.gov.in
†rmittal@barc.gov.in

crystallizes in four modifications. The β (monoclinic phase [42] with space group $P2_1/a$), γ (body-centered tetragonal phase [43], $I4_1/a$), and δ (monoclinic phase [44] with space group $P2_1/n$) phases are metastable; however, the only stable phase is known as α-$Na_2Si_2O_5$ (orthorhombic phase [45], *Pcnb*). X-ray-diffraction measurements, differential scanning calorimetry analysis, and electrochemical impedance spectroscopy show that the amorphous $Na_2Si_2O_5$ is metastable and transforms to a crystalline [46] form at around 773 K. The crystalline $Na_2Si_2O_5$ is observed to be a poor ionic conductor [41,46]. Moreover, the amorphous phase is structurally and electrically more stable in reducing atmosphere than in oxidizing ones. The presence of H or Al impurities in amorphous $Na_2Si_2O_5$ increases the crystallization temperature [46]. The ionic size of Na in $Na_2Si_2O_5$ is larger as compared to that of Li in $Li_2Si_2O_5$. However, the molecular dynamical simulations report [41,47] a lower activation energy in $Na_2Si_2O_5$ (0.3 eV) than that in $Li_2Si_2O_5$ (0.47 eV). The *ab initio* simulations [41] on amorphous $Na_2Si_2O_5$ show that Na preferentially diffuses within the layered channels formed by corner-shared SiO_4 tetrahedra.

The quasielastic neutron scattering (QENS) and molecular dynamics simulations are extensively used for studying the diffusion phenomenon at various length and timescale, for example diffusion of organic/inorganic solvents (or polymers) in various zeolites frameworks [48,49], dynamics of metal organic framework during adsorption of gases [50], and dynamics in molten salts [51]. The QENS spectra are measured as a function of temperature and momentum transfer. The spectroscopic technique enables study of the dynamics (segmental relaxation) of diffusing atoms or group of atoms following non-Debye and non-Arrhenius temperature dependence [49].

Further, QENS technique is also very well used to measure the dynamical motion of ions in materials [52]. In case of solid electrolyte, the technique was for the first time used to measure the ionic diffusion in β-alumina [53]. These experiments [53] revealed two types of diffusion mechanisms of Na at 400 °C, *viz.*, localized jumps and long-range diffusion. The QENS study of α-phase of Mg_3Bi_2 provides the mechanism of superionic diffusion of Mg^{+2} in the rigid bismuth lattice [54].

High Na ionic conductivity is desired for Na-ion batteries; however, there are very few materials which exhibit high Na ionic conductivity and most of them at well above room temperature. This paper deals with the possibility of getting high ionic conductivity by amorphization. Further, research is required to tune the ionic conductivity temperature by doping or another mechanism.

Recently, high-neutron flux of OSIRIS time of flight spectrometer at ISIS, United Kingdom has been used to measure Na-ion diffusion in sodium cobaltate [55]. Here we report microscopic analysis of Na-ion diffusion using state-of-the-art quasielastic neutron scattering measurements on a potential solid electrolyte material for Na battery. Such experimental studies are very sophisticated and rare due to low neutron scattering cross section of Na. There are only a few studies available in literature Ref. [55] and none on amorphous $Na_2Si_2O_5$. We have performed QENS measurements over a range of temperature from 300 to 748 K to evaluate the diffusion constant, nature, and pathways of Na-ion diffusion in the amorphous phase of $Na_2Si_2O_5$. To our knowledge there is no such microscopic analysis of diffusion mechanism of $Na_2Si_2O_5$, a potential new-generation energy material. The QENS measurements show a significant broadening of the elastic line beyond the resolution of the instrument.

In addition to the model-based analysis of QENS experiments to get detailed insight of Na-ion diffusion, the experimental studies are complemented by *ab initio* and force-field based molecular dynamics simulations (FF-MD) to provide a detailed atomic level understanding of the diffusion phenomena. Large-scale FF-MD simulations (1440 atoms) are performed on amorphous $Na_2Si_2O_5$ for over a few hundred picoseconds on large supercell (30-Å cell dimension gives $\sim$0.2-$Å^{-1}$ wave-vector transfer resolution comparable with experiments). Such large-scale simulations for a set of temperatures are extremely expensive with *ab initio* density-functional theory (DFT)-based molecular dynamics (AIMD), therefore, smaller-scale AIMD simulations are carried out. The AIMD calculations are free from any parametric force field and capture the polarizable nature interatomic forces important for ionic diffusion. Thus, this paper is providing deeper insight into the microscopic analysis of the diffusion mechanism in this material. The discrepancy obtained in diffusion coefficients between the model-based QENS analysis and molecular dynamics (MD) simulations are discussed in the paper. It is identified that finite-size effects in MD simulations and limitations in force-field approach are possible reasons. As discussed in the paper, we found that the AIMD are useful to understand the geometries of the diffusion pathways and their relaxation timescales, which is one of the important considerations of this work. In the amorphous phase various Na sites have been developed due to different orientations of silicon polyhedral units. The analysis of Na trajectories shows that some special Na sites provide pathways for Na diffusion, while these pathways are not available in crystalline phase. Thus, this work adds further knowledge in the microscopic analysis of diffusion and respective limitations of different methods, such as model-based QENS analysis, FF-MD, and AIMD

II. EXPERIMENTS

First, α-$Na_2Si_2O_5$ was synthesized [45] by conventional solid-state reaction between Na_2CO_3 and SiO_2 with four-step heating protocol. Silica (SiO_2, Alfa Aesar, 99.5%) powder was heated at 800 °C for 12 h in air and cooled to room temperature. Anhydrous Na_2CO_3 (Alfa Aesar, 99.9%) was heated at 200 °C for 2 hours and cooled to room temperature. Preheated Na_2CO_3 and SiO_2 in 1.05:1.0 molar ratio was thoroughly ground in acetone media and dried in air. The dried powder mixture was heated at 550 °C for 12 h and then reground. This *homogeneous* mixture was pelletized and heated at 650, 750, and 800 °C in air for 12 h at each temperature. The crystalline sample of α-$Na_2Si_2O_5$ was obtained after heating at 800 °C for 12 h. The amorphous $Na_2Si_2O_5$ was prepared by melt-quench method. Pellets of crystalline α-$Na_2Si_2O_5$ were crushed to powder form, and filled into a platinum crucible. The crucible with sample was heated to 950 °C at a heating rate 2 °C/min and held for 4 h in a muffle furnace. The sample was removed from the

furnace by sliding the sample stage of the furnace. The melted sample was quenched by immediately dropping the platinum crucible along with the sample to a container filled with liquid nitrogen. The transparent solidified melt was separated from crucible mechanically and stored in a vacuum desiccator. The obtained transparent glass sample pieces were finely ground to powder and characterized by x-ray diffraction.

The QENS measurements were performed on amorphous Na_2SiO_5 using the OSIRIS [56–58], the indirect geometry time of flight spectrometer at ISIS. The final energy in the measurements was fixed at 1.84 meV using pyrolytic graphite (002) analyzers, giving the energy resolution of 25.4 μeV. Scattered neutrons were detected over an angular range of $2\theta = 25^\circ - 160^\circ$, providing available Q range $0.42 - 1.85\,\text{Å}^{-1}$. The amorphous polycrystalline powder samples were kept in a niobium sample holder and sealed. A high-temperature furnace operating in high vacuum served as the sample environment. The experimental data on sample have been recorded at several temperatures from 300 to 773 K. The data taken on empty niobium sample holder are used to remove the background scattering due to the sample environment. A vanadium standard was measured for normalization of detectors and for measuring the resolution of the instrument. The data as collected in various detectors were grouped in the wave-vector (Q) steps of $0.05\,\text{Å}^{-1}$ for improving the counting statistics. The experimental data were normalized and corrected for detector efficiency and detailed balance using the standard program package for data analysis available at the spectrometer. All data analyses were performed using the QENS data analysis interface as implemented in MANTID software [59,60].

III. CALCULATIONS

The molecular dynamics simulations of the diffusion process are carried out using both the *ab initio* density-functional theory and force-field approach based on interatomic potentials. These two approaches were necessary since the DFT simulations can only be performed, even on supercomputers available to us, on a rather small simulation cell that may limit the pathways of the diffusion process, while the force-field simulations could be performed on much larger cells and also for much longer time duration. We have also performed the lattice dynamics calculations using both the approaches to evaluate the phonon spectrum. As the results from the two approaches are found to be consistent with each other, we have used the larger simulations to visualize the geometries of the diffusion pathways and their timescales.

For the force-field simulations, we have used the Buckingham model of interatomic potential, which consists of long-range Coulomb interaction, short-range repulsive interaction, and van der Waals interaction terms, given by

$$V(r) = \frac{e^2}{4\pi\varepsilon_o}\frac{Z(k)Z(k')}{r} + a\,\exp\left[\frac{-br}{R(k)+R(k')}\right] - \frac{C}{r^6}, \tag{1}$$

where r is the separation between the atoms of type k and k', and $R(k)$ and $Z(k)$ are, respectively, the effective radius and charge of the kth atom. As in earlier studies, $a = 1822\,\text{eV}$ and $b = 12.364$ have been treated as constants. This choice has been successfully used earlier to study the phonon properties of several complex solids [61,62]. The optimized parameters as used in our calculations are $Z(\text{Na}) = 1.0$, $Z(\text{Si}) = 2.6$, $Z(\text{O}) = -1.44$, $R(\text{Na}) = 1.07\,\text{Å}$, $R(\text{Si}) = 0.70\,\text{Å}$, $R(\text{O}) = 2.09\,\text{Å}$. The van der Waals interaction ($C = 50.0\,\text{eV Å}^6$) is introduced only between the oxygen atoms. The phonon calculations in the α-$Na_2Si_2O_5$ are performed using the software [63] developed at Trombay.

The force field molecular dynamics simulations have been performed on a super cell size of $4 \times 5 \times 2$ (1440 atoms) for 200 ps after the equilibration. The simulations are carried out in NPT ensemble. To create the amorphous phase, we have melted the crystalline phase at 2500 K in 10 ps and then quenched to 10 K over 250 fs. Further, after the quenching at 10 K, the simulation was continued for 300 ps to ensure that there is no drift in the total energy or temperature due to strain in the amorphous structure. To characterize the phases, we have performed simulations at 300 K in both the crystalline and amorphous phases for 200 ps after equilibration. The quench rate used in our simulations appears to be reasonable, which is similar to that in previous literature [41]. The simulations in both the crystalline and amorphous phases have been performed at various temperatures from 300 to 1200 K using DL_POLY software [64]. The mass density of the crystalline and amorphous phases is 2.52 and 1.71 gm/cc, respectively, at 10 K.

To perform *ab initio* density-functional theory based phonon calculation we have used the Vienna *Ab initio* Simulation Package [65,66] (VASP). The supercell scheme has been used for phonon calculation, i.e., the forces on various atoms have been calculated on a $2 \times 2 \times 1$ supercell of dimension. The supercell and subsequent atomic displacements have been generated using PHONOPY software [67]. Further, the forces and displacement of different configuration have been used to calculate the phonon spectrum using PHONOPY software. The total energy and forces calculation using VASP are performed using the projected augmented-wave formalism of the Kohn-Sham density-functional theory within generalized gradient approximation for exchange correlation following the parametrization by Perdew, Burke, and Ernzerhof [68,69]. The plane-wave pseudopotential with a plane-wave kinetic energy cutoff of 700 eV was adopted. The integration over the Brillouin zone is sampled using a k-point grid of $6 \times 6 \times 2$, generated automatically using the Monkhorst-Pack method [70]. The total energy is minimized with respect to structural parameters. The convergence criteria for the total energy and ionic forces were set to $10^{-8}\,\text{eV}$ and $10^{-4}\,\text{eV Å}^{-1}$, respectively.

For *ab initio* molecular dynamics simulation, we have taken a single k point in the Brillouin zone. An energy convergence of $10^{-6}\,\text{eV}$ has been chosen for self-consistence convergence. A time step of 2 fs is used. The amorphous structure in the *ab initio* method has been generated using the following steps. We started with the crystalline $Na_2Si_2O_5$ phase (216 atoms, $2 \times 3 \times 1$ supercell of the orthorhombic phase) and melted it using *ab initio* molecular dynamics simulation at 2500 K for 10 ps. Then we quenched the structure to 10 K and used the quenched structure as an amorphous structure of $Na_2Si_2O_5$. The quenching rate used is similar

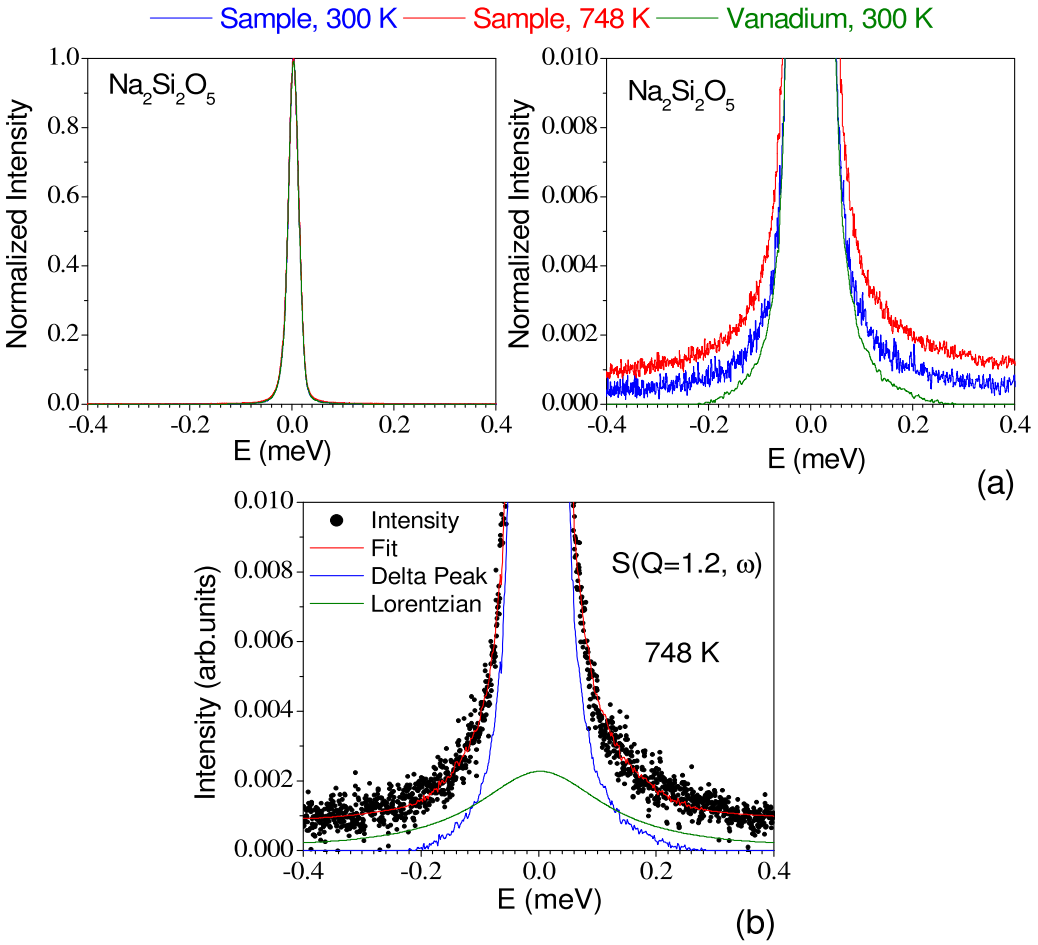

FIG. 1. (a) Comparison of as observed dynamical neutron-scattering function $S(Q,\omega)$ of amorphous $Na_2Si_2O_5$ integrated over all Q at 300 K (blue line) and 748 K (red line) and the instruments resolution (vanadium at 300 K; green line). The data have been normalized to unity at the peak position. (b) Fit of one Lorentzian peak and one delta function convoluted with the resolution function at a selected $Q = 1.2\,\text{Å}^{-1}$ slice of $S(Q,\omega)$, and a linear background.

to that in previous literature [41]. Simulations are performed for a series of temperatures from 300 to 1100 K. Initially, the structure was equilibrated for 10 ps to attain the required temperature in NVT simulations through a Nosé thermostat [71]. Then for the production runs up to 40 ps, NVE simulations are performed. At each temperature, a well-equilibrated configuration is observed during the 40-ps simulation.3

The isotropic diffusion coefficient can be estimated from the time dependence of mean-square displacement as given below:

$$D = \langle u^2 \rangle / 6\tau, \tag{2}$$

where $\langle u^2 \rangle$ is the change in the mean-square displacement (MSD) in time τ. The MSD at time τ is calculated using the following equation [22,72]:

$$u^2(\tau) = \frac{1}{N_{\text{ion}}\left(N_{\text{step}} - N\tau\right)} \sum_{i=1}^{N_{\text{ion}}} \sum_{j=1}^{N_{\text{step}}-N_\tau} |r_i(t_j + \tau) - r_i(t_j)|^2. \tag{3}$$

Here $r_i(t_j)$ is the position of the ith atom at the jth time step. N_{step} is total number of simulation steps and N_{ion} is total number of atoms of a particular type in the simulation cell. $N_\tau = \tau/(\delta t)$, where δt is step size.

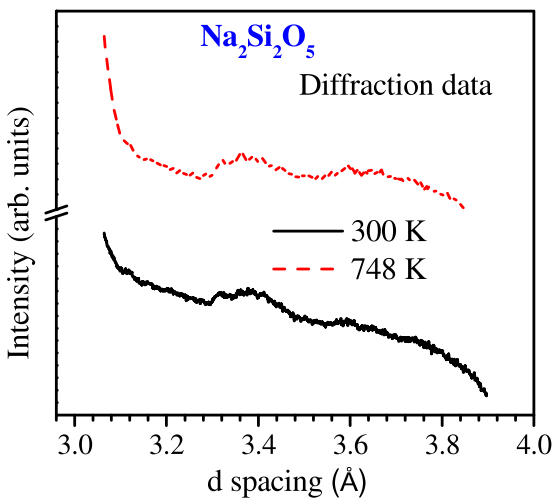

FIG. 2. The integrated intensity as a function of d spacing at 300 and 748 K.

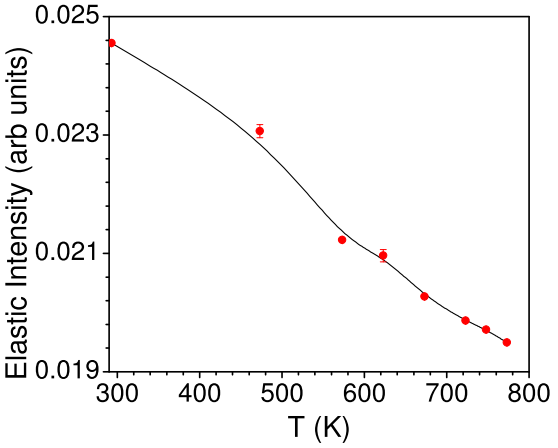

FIG. 3. Temperature-dependent variation of integrated elastic peak intensity extracted from dynamic neutron-scattering function $S(Q,\omega)$. The data are summed over all Q.

IV. RESULTS AND DISCUSSION

A. Quasielastic neutron scattering

QENS is a powerful experimental technique, which enables us to measure diffusion process. It exhibits the broadening of the elastic scattering caused by nonperiodic "diffusive motion" in the sample as a function of momentum transfer. The quasielastic signal in neutron-scattering experiments contains the sum of coherent and incoherent contributions. The information from QENS is unique in the sense that this could provide microscopic information about the diffusion, such as providing simultaneously the jump length and residence time, which other techniques do not. These two quantities are very important to design the materials for ionic diffusion. In case of $Na_2Si_2O_5$, silicon and oxygen only scatter coherently; the incoherent contribution is dominant by the scattering from sodium. Sodium has nearly identical coherent and incoherent cross sections [73]. The dynamical motion of Na diffusion using QENS experiments in this potential battery material is challenging due to low neutron-scattering cross section of Na [73], and the data interpretation is also difficult due to the coherent nature of the scattering from Na atom.

Figure 1 shows comparison of the dynamic neutron-scattering function $S(Q,\omega)$ of amorphous $Na_2Si_2O_5$ integrated over all Q and at 300 and 748 K and instrument's resolution. The measurements at 748 K provide clear evidence of the QENS broadening. The data at 748 K can be fitted to one Lorentzian peak and one delta function convoluted with the resolution function of the instrument, providing evidence of QENS broadening from the sample. The diffraction data (Fig. 2) on the same temperature at 300 to 748 K shows that in vacuum, we did not found any evidence for crystallization

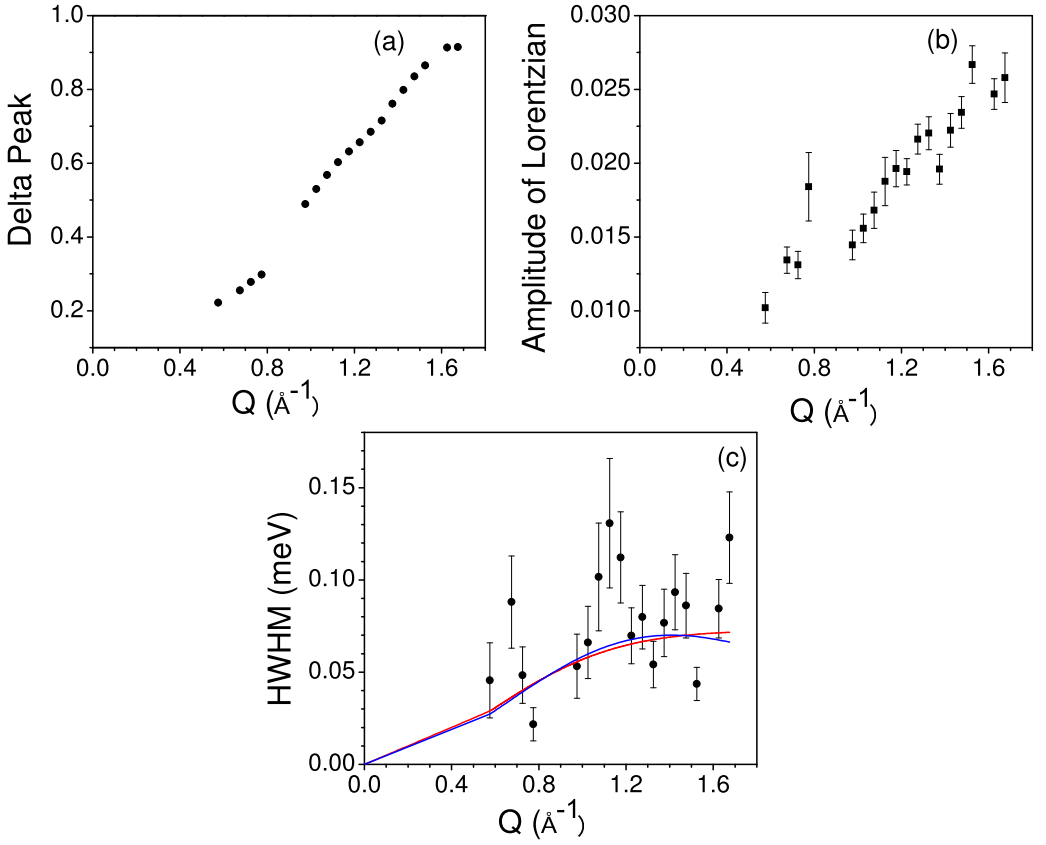

FIG. 4. Q-dependent variation of (a) elastic peak height, (b) amplitude of Lorentzian, and (c) and half width at half maximum of Lorentzian peak extracted from dynamic neutron-scattering function $S(Q,\omega)$ of amorphous $Na_2Si_2O_5$ at 748 K in vacuum. Q binning is done in steps of 0.05 Å^{-1}. The solid red lines in (c) are obtained from the fits of the Hall-Ross (red line) and Chudley-Elliott (blue line) models to the experimental data.

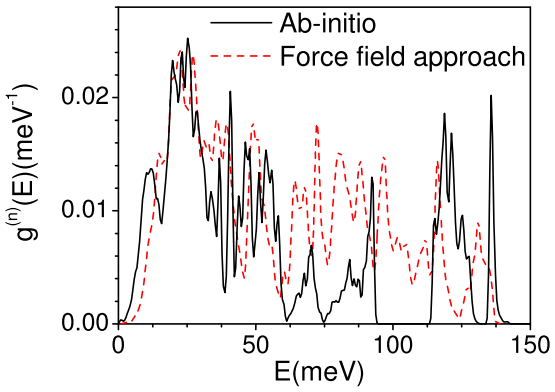

FIG. 5. The calculated phonon density of states of $Na_2Si_2O_5$ in orthorhombic phase using *ab initio* density-functional theory method and force-field approach.

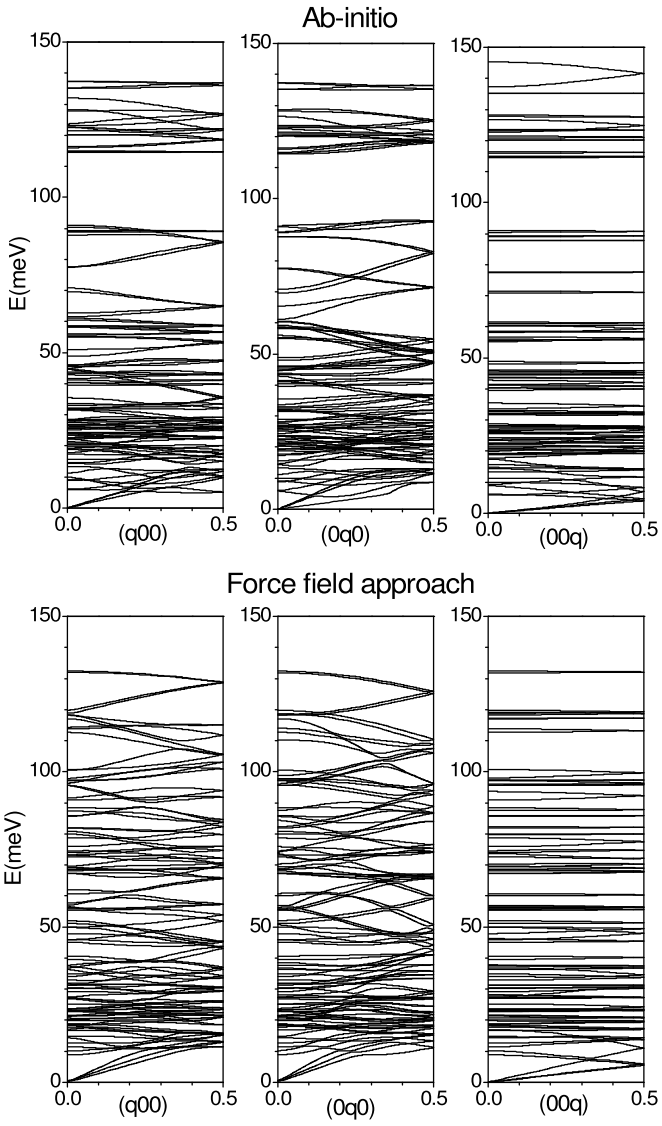

FIG. 6. The calculated phonon dispersion relation of $Na_2Si_2O_5$ in orthorhombic phase using *ab-initio* density-functional theory method and force-field approach.

of sample and provide evidence that the sample remains in the amorphous phase in the entire temperature range of our measurements. The temperature-dependent variation of elastic intensity extracted from dynamic neutron-scattering function summed over all Q is shown in Fig. 3, which does not show any sudden drop of elastic intensity. This is consistent with the fact that there is no phase change in the solid at the experimental temperature range. However, from Fig. 3, the change in elastic intensity is more than that expected from only the Debye-Waller factor, which could be due to increase in disorder [74].

Further, in order to understand the microscopic nature of sodium diffusion we need Q dependence of quasielastic broadening. The data collected in various detectors in the Q range from 0.6 to 1.7 $Å^{-1}$ were grouped in the Q steps of 0.05 $Å^{-1}$. The individual data in steps of 0.05 $Å^{-1}$ are fitted to one Lorentzian peak and one delta function convoluted with the resolution function of the instrument. All the fits were done over an energy range $-0.4 \leqslant E \leqslant 0.4$ meV, chosen to be symmetric around $E = 0$. The Q-dependent variation of elastic peak height, amplitude, and width of Lorentzian peak extracted from dynamic neutron-scattering function is shown in Fig. 4. It can be seen that peak height of elastic and amplitude of Lorentzian peak [Fig. 4(b)] increase with increasing Q. The monotonic increase in intensity of the elastic contribution with Q over 0.6 to 1.7 $Å^{-1}$ might be partially due to the amorphous structure and partially due to coherent scattering. However, width of Lorentzian peak which gives information about the diffusion (quasielastic linewidth) shows a significant Q dependence and indicates increment of the diffusion process.

The Q dependence of half width at half maximum (HWHM) is fitted using the Hall and Ross (H-R) model [75,76] as well as the Chudley-Elliott (C-E) model [77], which are appropriate models for variable length jump-diffusion process. The C-E model assumes a fixed value of the jump length (d). On the other hand, the H-R model assumes that the jump lengths are distributed and a root-mean-squared value of the jump length is used to fit the experimental data. In case of H-R model [75,76], the Q dependence of HWHM [(Q)] is related to the jump length (d) and average jump time (τ) from one site to another site by the following expression:

$$\Gamma(Q) = (1 - \exp(-\langle d^2 \rangle Q^2/6))/\tau. \quad (4)$$

Similarly, for the Chudley-Elliott model [77] the corresponding expression is given by

$$\Gamma(Q) = [1 - \sin(Qd)/Qd]/\tau. \quad (5)$$

Figure 4(c) shows the Q dependence of the QENS broadening with a fit of the H-R and C-E models of jump diffusion for amorphous $Na_2Si_2O_5$ at 748 K. The fit of the H-R model to QNES data gives a mean residence time 9.1 $\pm$ 1.4 ps ($13.8 \pm 2.2\,meV^{-1}$) and diffusion jump length of 3.0 $\pm$ 0.8 Å, which give a diffusion coefficient of $(16 \pm 11) \times 10^{-10}\,m^2/s$. Similarly the Chudley-Elliott model gives τ and d values of 11.4 $\pm$ 1.2 ps ($17.4 \pm 1.8\,meV^{-1}$) and 3.2 $\pm$ 0.5 Å, respectively, resulting in diffusion coefficient value of $(15 \pm 6) \times 10^{-10}\,m^2/s$. As expected, the jump length as estimated from the fits of the experimental data matches very

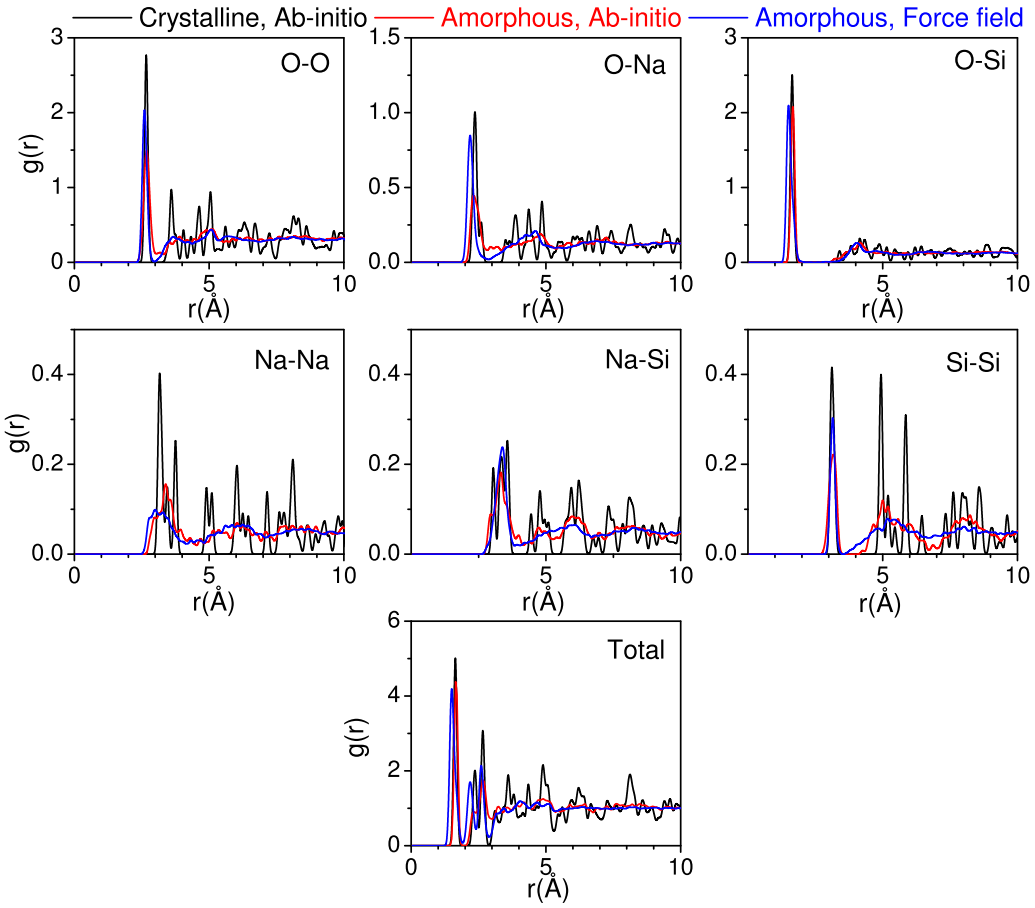

FIG. 7. The calculated pair-distribution functions of various pairs of atoms in crystalline and amorphous phase of $Na_2Si_2O_5$ using *ab initio* and force-field MD approach.

well with the calculated first-neighbor distance of 2.98 Å in the amorphous phase (discussed below). It is clear from Fig. 4(c) that there is considerable scatter of the data points. Consequently, there are large error bars on the jump lengths, jump time, and diffusivity determined from the QENS data. In view of these shortcomings, molecular dynamics simulations were performed in order to get more information on the diffusion process.

B. Molecular dynamics simulations

The magnitude of broadening at a particular wave-vector transfer in the QENS peak depends on the diffusion coefficient of the diffusive species; in our case it is Na ion. The quasielastic broadening as observed from experiment gives quantitative estimate of the diffusion coefficient. However, the nature of diffusion and microscopic view may not be completely inferred from the experiment. Hence, in order to get the insight of Na-ion diffusion, we have performed simulation in the amorphous phase of $Na_2Si_2O_5$ compound. In order to simulate the quasielastic broadening with appropriate momentum resolution, the simulation is performed for few hundred picoseconds on a large supercell (30-Å cell dimension gives $\sim$0.2-$Å^{-1}$ momentum transfer resolution). Such a big scale simulation for a set of temperatures is extremely expensive with AIMD method and can be achievable with FF-MD methods. The main challenge of force-field methods is a good set of force-field parameters, which can be used for calculation of thermodynamical and transport properties. Further, we have also performed the *ab initio* molecular dynamics simulation in the amorphous phase of $Na_2Si_2O_5$.

The amorphous structure of $Na_2Si_2O_5$ consists of randomly oriented SiO_4 tetrahedral units stuffed with Na. In order to optimize the force-field parameter of the Buckingham potential, we have performed rigorous calculations with various sets of parameters. We have tested several sets of parameters and chosen the set of parameters which reproduces the closest experimental structure and phonon dynamics as obtained from DFT calculations (Figs. 5 and 6) in the α-$Na_2Si_2O_5$. The comparison of the experimental lattice parameters with that obtained from *ab initio* and force-field approach calculations (Table I) show differences of about 3–4%, which is quite satisfactory. The calculated phonon density of states and phonon dispersion from both the approaches are shown in Figs. 5 and 6, respectively. The maximum of the phonon frequencies from both the approaches is quite similar at about 140 meV. The phonon spectrum as calculated from the interatomic potential, up to about 95 meV, is qualitatively in fair agreement with *ab initio* phonon density of states. However, we find that the in the *ab initio* calculated phonon spectrum, there is a phonon band gap around 95–115 meV, while in the force-field approach there is no such phonon

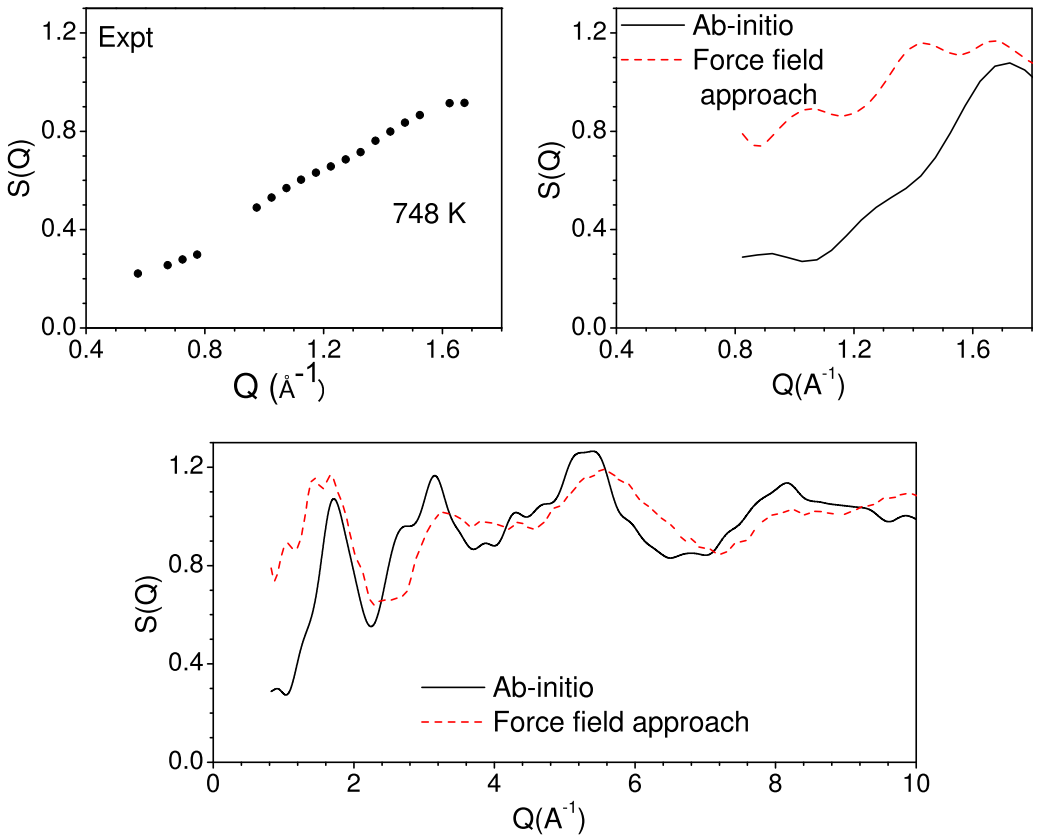

FIG. 8. The comparison between the calculated and experimental $S(Q)$ in amorphous phase. Bottom panel gives the calculated $S(Q)$ from *ab initio* and force-field approach up to $Q = 10$ Å^{-1}.

band gap. This might be due to the fact that the oxygen polarizability is not taken care in our force-field model. In order to include all these effects, the force-field model required more parameters and would not be suitable for very large simulations. It should be noted that the thermodynamic behavior of compounds is largely dominated by low-energy spectrum of phonon. Hence the optimized set of force-field parameters can be further used in the FF-MD simulations to investigate the dynamics of atoms at high temperatures.

The computed time-averaged pair-distribution functions [$g(r)$] of various pairs of atoms in $Na_2Si_2O_5$ are shown in Fig. 7 in the amorphous and crystalline phases at 300 K. It can be seen that total pair distribution function (PDF) among atoms using the two approaches of *ab initio* and force-field model show fair agreement with each other. We found that the crystalline structure consists of sharp and well-defined peaks at various bond lengths representing its long-range order, while in the amorphous phase the sharp peak is seen only for the short-range order of the first neighbors, as expected in amorphous solids [78]. It shows that Si-O PDF intensity for the first-neighbor distance ∼1.6 Å does not change much between the crystalline and amorphous phase, while other higher neighboring peaks show significant change. This is due to the fact that the polyhedral unit of SiO_4 does not change its shape, while its orientation (medium-range order) changes significantly in the amorphous phase. Further, the Na-Na PDF intensity changes significantly in the amorphous structure with respect to the crystalline structure even for the short-range order, which signifies that the Na distribution changes significantly between the crystalline and amorphous phases. The broad structures at higher distance are attributed to the broad distributions of interatomic distances in medium and long range, which indicate a well-constructed amorphous structure. We have performed further analysis with this configuration.

TABLE I. The experimental [45] and calculated structural parameters of orthorhombic $Na_2Si_2O_5$ (space group *Pcnb*) using *ab initio* and force-field model.

	Expt. (300 K)	*Ab initio* (0 K)	Force-field model (0 K)
a (Å)	6.408 99	6.436	6.183
b (Å)	4.895 99	4.945	5.133
c (Å)	15.422 0	15.570	15.112

As noted above, the calculated $g(r)$ from the AIMD and FF-MD simulations in Fig. 7 are in fair agreement with each other. In Fig. 8 we show the structure factor $S(Q)$ from the *ab initio* and FF-MD simulations, which are also in fair agreement with each other. We also show in Fig. 8 the comparison between the simulated and experimental $S(Q)$, which is quite satisfactory. We have compared the experimental $S(Q)$ data rather than the derived $g(r)$, since the Q range in the experimental QENS data is limited to 1.7 Å^{-1}, not sufficient to derive $g(r)$.

The force-field as well as *ab initio* molecular dynamics simulations have been performed at various temperatures from 300 to 1100 K. Further, we have analyzed the

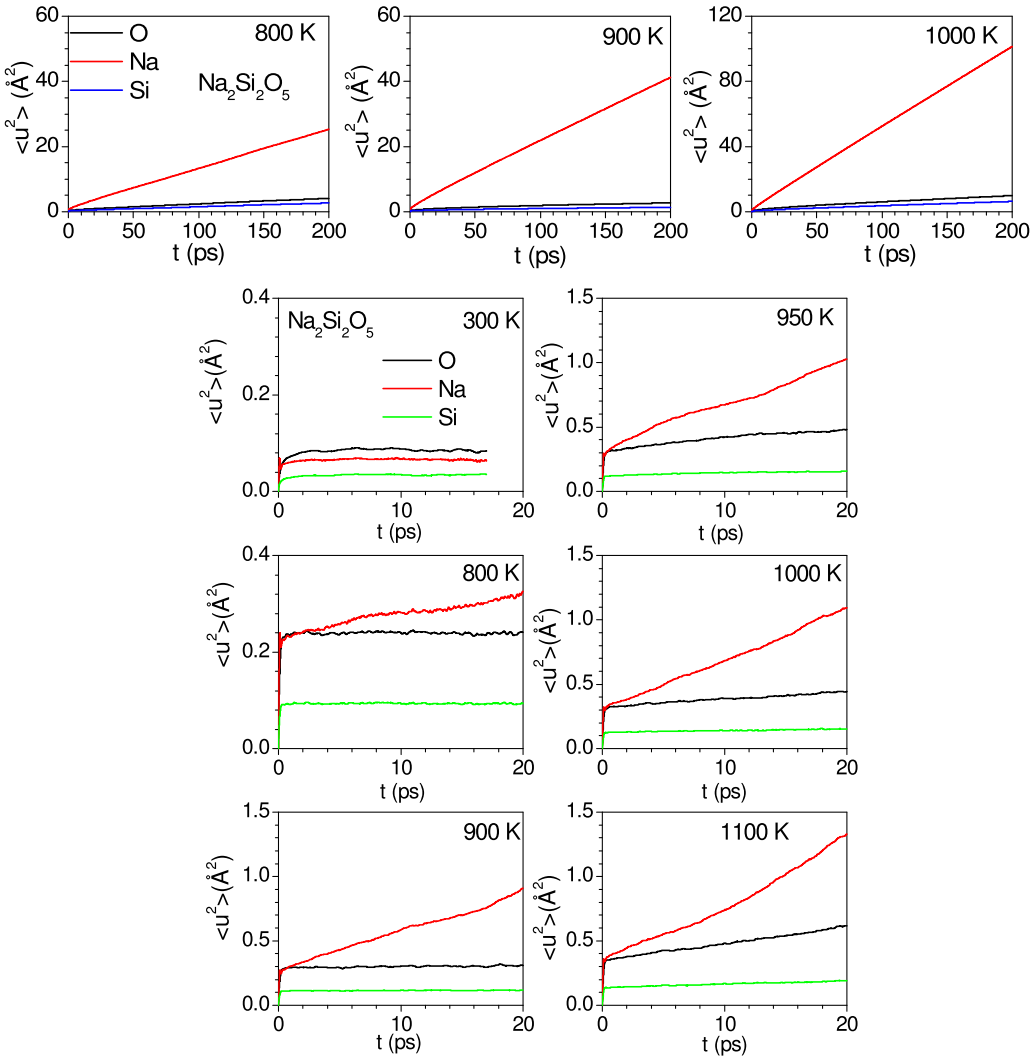

FIG. 9. The calculated mean-squared displacement of various atoms in amorphous phase of $Na_2Si_2O_5$ using force-field (top panel) and *ab initio* (bottom panel) MD simulations.

mean-squared displacement of various atoms in the crystalline and amorphous phase. It is interesting to note that the diffusion in $Na_2Si_2O_5$ occurs only in the amorphous phase while the crystalline phase does not show any diffusion up to 1100 K. We found that the MSD of Na atoms shows significant time dependence at and above 800 K in the amorphous phase, while in the crystalline phase even up to 1100 K there is insignificant variation of MSD with time. This gives a signature that in the amorphous phase significant diffusion occurs at and above 800 K while there is no diffusion in the crystalline phase.

In Fig. 9, we have shown the MSD obtained from *ab initio* and force-field molecular dynamics simulation in the amorphous phase at various temperatures. The mean-squared displacements of various atoms have been calculated using Eq. (3). We found that the mean-squared amplitude of Na atoms keeps increasing with time, which is a signature of the diffusion of Na atoms in the compound (Fig. 9). The mean-squared displacement of other atoms, Si and O, does not show any increase with time; hence, there is no significant diffusion of these atoms, which is essential for a stable solid electrolyte. The diffusion coefficient as estimated from *ab initio* calculations (on a 216-atom cell) is smaller in comparison to that from the force-field calculations (on a 1440-atom cell) (Fig. 10). This might be due to the finite-size effect in molecular dynamics simulation. As discussed below, we found that the *ab initio* simulations are useful to visualize the geometries of the diffusion pathways and their timescales, which is one of the important considerations of this work.

The time dependence of mean-squared displacement of various atoms has been used to estimate the diffusion coefficient (Fig. 9). The calculated diffusion coefficients at various temperatures as estimated from *ab initio* and force-field molecular dynamics simulation are shown in Fig. 10. The energy barrier for sodium diffusion can be estimated from the fitting of the temperature dependence of diffusion coefficients with Arrhenius relation, i.e.,

$$D(T) = D_0 \exp(-E_a/K_B T). \tag{6}$$

One can linearize this equation by taking log of it, i.e.,

$$\ln[D(T)] = \ln(D_0) - E_a/K_B T. \tag{7}$$

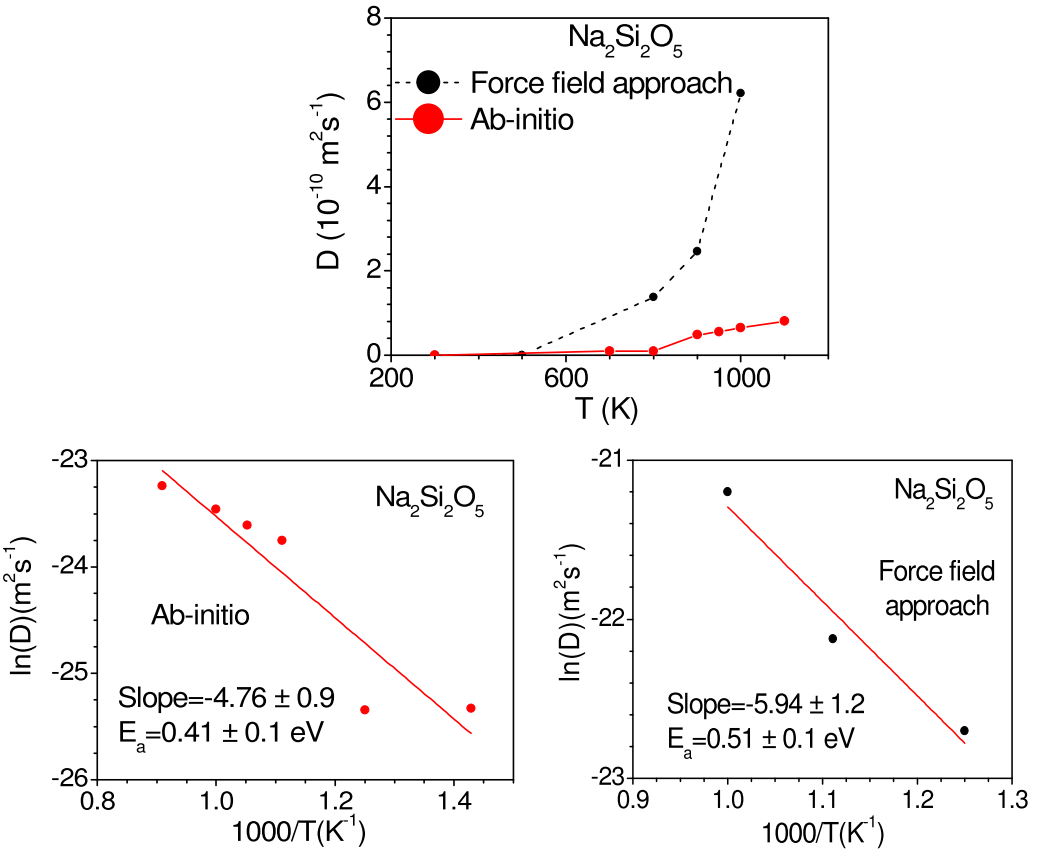

FIG. 10. The calculated diffusion coefficients and activation energy barriers in amorphous phase of $Na_2Si_2O_5$ as estimated using force-field and *ab initio* molecular dynamics simulations.

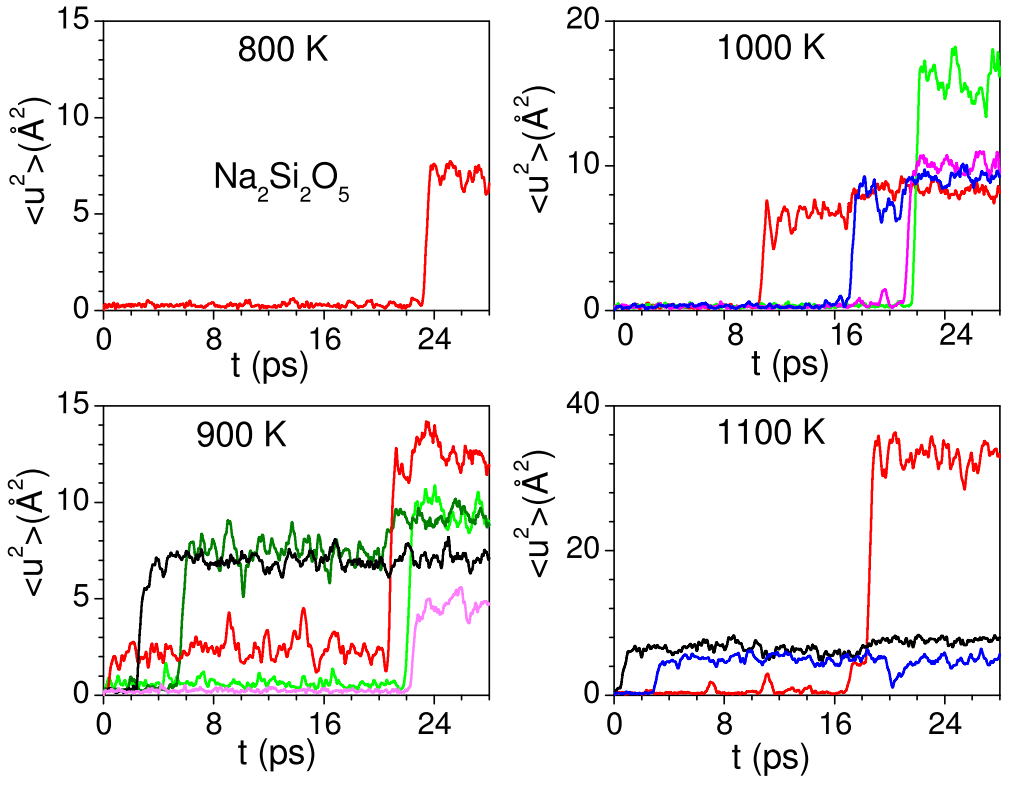

FIG. 11. The calculated displacement of Na atoms in $Na_2Si_2O_5$ as estimated using *ab initio* molecular dynamics simulations.

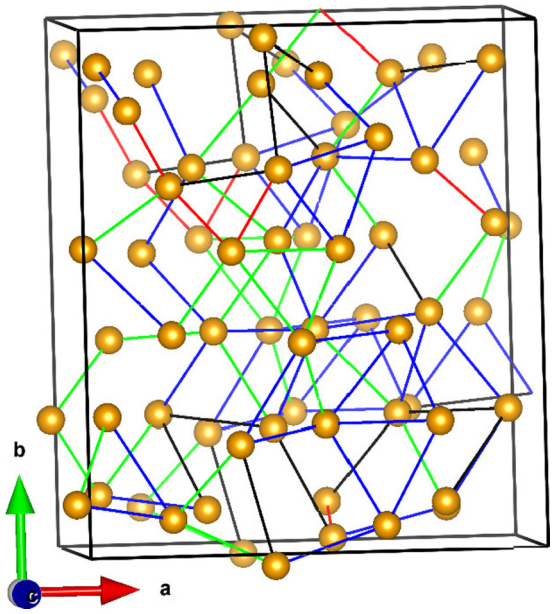

FIG. 12. The distribution of 48 Na atoms in the amorphous phase, depicted in the *ab initio* simulation cell. The color of the bond joining any two Na atoms represents the distance between them (red = 2.7−3.0 Å; green = 3.0−3.3 Å; blue = 3.3−3.6 Å; black = 3.6−3.9 Å).

Here D_0 is the constant factor, K_B is the Boltzmann constant, and T is temperature. We have fitted the simulation data to Eq. (7) in Fig. 10 for the force-field and *ab initio* MD simulations and the value of the activation energy is found to be 0.51 ± 0.1 eV and 0.41 ± 0.1 eV from force-field and *ab initio* MD simulations, respectively.

The estimated diffusion coefficients (Fig. 10) show very small diffusion up to 800 K, and above that the diffusion coefficient shows a huge jump. To understand how the Na-ion diffusion coefficient increases with temperature, we have plotted the mean-squared displacement of individual Na atoms (Fig. 11). We observe that a few Na atoms show sudden jump in the mean-squared displacement, which essentially indicates a jumplike diffusion of Na atoms in the amorphous phase. At 800 K, only a few Na atoms show jump in MSD with a jump length of ∼2 Å; however, at above 900 K, significant number of Na atoms show jump in MSD. Further, the jump length shows a distribution from ∼1.4 to 3 Å. This distribution of the jump lengths is a consequence of the amorphous structure of materials where we have an irregular spatial distribution of Na atoms. In Fig. 12, we have shown the distribution of Na-Na distance in the amorphous structure with different magnitude of bond length denoted by a different color. We can see how the Na atomic sites are connected in the amorphous phase and provide the pathways for diffusion. Further, it may be noticed that even the same path length may not result in the same activation energy, since for the same path length the ionic trajectory for Na hopping may be different. which depends on the local site environment.

The calculated trajectories of various atoms from the *ab initio* MD simulation in the amorphous phase are shown in Fig. 13. We find that the Na atoms move from one site to another via jumplike diffusion, and the number of Na atoms participating in jump diffusion as well as jump frequency increases significantly with temperature. The increase in the number of Na atoms and jump frequency is gradual, which might be due to the fact that in the amorphous phase the distances between two Na sites are not unique and show a distribution.

In order to gain microscopic understanding of the diffusion behavior from quasielastic broadening as obtained from neutron data, we have computed incoherent dynamical structure factor [48] $S(Q, \omega)$ at allowed wave-vector Q values at 1000 K. The lowest Q value of 0.2 $Å^{-1}$ in the calculations is limited by the size of the super cell. The calculated dynamical incoherent structure factors $S(Q, \omega)$ are fitted with the single Lorentz peak function

$$S(Q, \omega) = A\frac{\Gamma}{\Gamma^2 + \omega^2}. \tag{8}$$

Here A is the normalization constant and Γ is half width at half maximum energy.

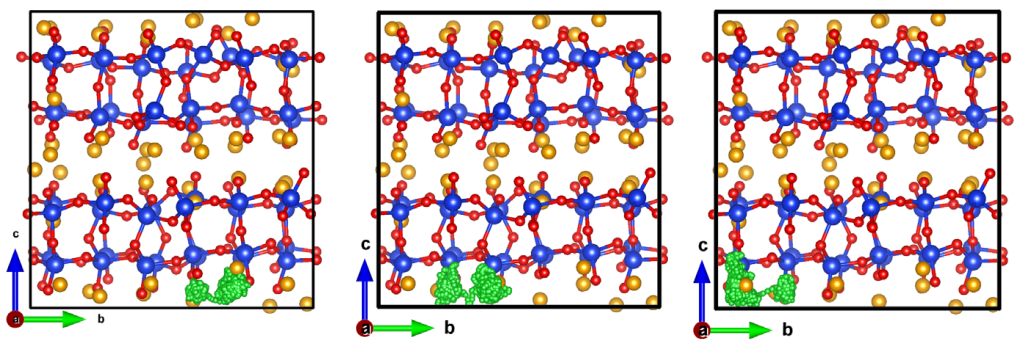

800 K, (0.936 0.739 0.094) **900 K, (0.792 0.252 0.040)** **900 K, (0.950 0.062 0.071)**

FIG. 13. The observed trajectories of selected Na atoms in *ab initio* MD simulations at 800 and 900 K in $Na_2Si_2O_5$ as projected in the *b*-*c* plane. All the atoms (key: Na- yellow sphere; Si- blue sphere; O- red sphere) are also shown at their respective position in the beginning of the simulation. The time-dependent positions of the selected Na atoms are shown by green colored dots. The numbers below each frame indicate the temperature of the simulation and atomic fractional coordinate of the selected Na atom at the beginning of the *ab initio* simulation. The fractional coordinate values are given with respect to the simulation cell.

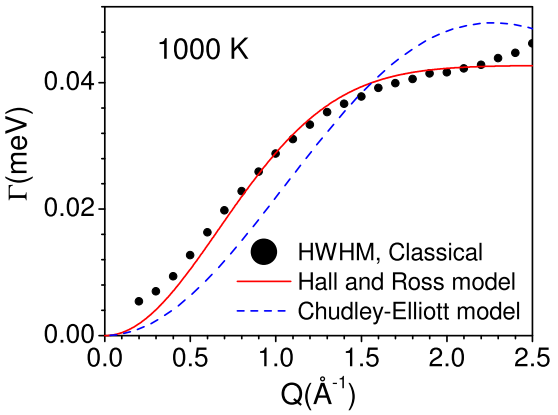

FIG. 14. The calculated wave-vector dependence of HWHM of dynamical incoherent structure factor of Na atoms in amorphous phase of $Na_2Si_2O_5$ using force-field MD approach at 1000 K and fitted with H-R and C-E models.

The calculated HWHM is plotted as a function of wave vector Q at 1000 K [$\Gamma(Q,T)$] for amorphous phase of $Na_2Si_2O_5$ (Fig. 14). This contains the information about the diffusion behavior in space and time. In amorphous phase the Na atoms jumps from one position to another and it is expected to not be a continuous diffusion as there is no unique jump length in the amorphous structure.

As shown above, both the H-R model and Chudley-Elliott model fit experimental data fairly well. However, our simulated quasielastic broadening with Q fits (Fig. 14) well with H-R model [Eq. (4)] of jump diffusion. The fitting using H-R model gives a jump length of about 2.6 ± 0.1 Å at 1000 K and residence time of 15.4 ± 0.2 ps ($23.4 \pm 0.3\,\mathrm{meV}^{-1}$). The jump length matches very well with that obtained from the experimental data of 3.0 ± 0.8 Å and also the first-neighbor distance (Fig. 7) in the amorphous structure (∼2.98 Å), although the residence time is longer than that obtained from the experiments values of 9.1 ± 1.4 ps ($13.8 \pm 2.2\,\mathrm{meV}^{-1}$). The diffusion coefficient value as estimated using H-R model from calculations at 1000 K is $7.3 \pm 0.4 \times 10^{-10}\,\mathrm{m}^2/\mathrm{s}$, while the corresponding value from QENS data at 748 K is $(16 \pm 11) \times 10^{-10}\,\mathrm{m}^2/\mathrm{s}$.

The discrepancies in the relaxation time obtained from FF-MD, AIMD, and QENS models can be explained by noting the limitations of various methods in calculating the diffusion coefficients. Both FF-MD and AIMD suffer the limitation of finite size of the cells of the amorphous $Na_2Si_2O_5$. The calculations with AIMD are limited by the smaller size of the simulations cells in comparison of the cell size in FF-MD. On the other hand, the force-field model of the FF-MD is limited by its potential, which is not polarizable as mentioned above. The model-based analysis of QENS data has its own limitation. Irrespective of these challenges, the current work shows that even in a small size of the simulation cell, the amorphous structure of $Na_2Si_2O_5$ has been expressed correctly in AIMD calculations. The jump lengths are also independent of the method of analysis. This method of analysis thus can be applied to other amorphous materials of this kind. More work on the dependence of relaxation time on cell sizes will be presented later.

V. CONCLUSIONS

Here we have reported the quasielastic neutron-scattering measurements of the amorphous $Na_2Si_2O_5$ as a function of temperature. The quasielastic energy width as a function of momentum transfer has been fitted to jumplike diffusion models (H-R model and C-E model) of the Na ions with a typical jump length of about 3 Å and residence time of about 10 ps. The molecular dynamics simulations have provided further insight of the diffusion mechanism; the simulations show that there is a distribution of jump lengths centered around 2.6 Å. The analysis of Na trajectories shows that in the amorphous phase various Na sites have been created due to misorientation of silicon polyhedral units and some of them are connected and provide a pathway for Na diffusion, while these pathways were not available in crystalline phase. It is also shown that jump lengths obtained from different methods of analysis, FF-MD, AIMD, analytic model-based QENS analysis agreed well; however, AIMD underestimated relaxation time with respect to FF-MD and the model-based analysis.

ACKNOWLEDGMENTS

The use of ANUPAM supercomputing facility at BARC is acknowledged. The authors thank the Department of Science and Technology, India (Grant No. SR/NM/Z-07/2015) for the financial support and Jawaharlal Nehru Centre for Advanced Scientific Research (JNCASR) for managing the project. The authors also thank STFC, UK for the beam-time at ISIS (Experiment No. RB1910264 on OSIRIS) and also availing the travel support from the Newton fund, ISIS, UK. S.L.C. thanks the Indian National Science Academy for award of an INSA Senior Scientist position.

[1] J.-H. Lee, J. Kim, T. Y. Kim, M. S. Al Hossain, S.-W. Kim, and J. H. Kim, J. Mater. Chem. A **4**, 7983 (2016).
[2] X. Luo, J. Wang, M. Dooner, and J. Clarke, Appl. Energy **137**, 511 (2015).
[3] M. R. Lukatskaya, B. Dunn, and Y. Gogotsi, Nat. Commun. **7**, 12647 (2016).
[4] H. Sun, Y. Zhang, J. Zhang, X. Sun, and H. Peng, Nat. Rev. Mater. **2**, 17023 (2017).
[5] K. C. Divya and J. Ostergaard, Electr. Power Syst. Res. **79**, 511 (2009).
[6] W. Zhou, Y. Li, S. Xin, and J. B. Goodenough, ACS Cent. Sci. **3**, 52 (2017).
[7] J. B. Goodenough and K.-S. Park, J. Am. Chem. Soc. **135**, 1167 (2013).
[8] D. Larcher and J. M. Tarascon, Nat. Chem. **7**, 19 (2015).
[9] M. H. Braga, N. S. Grundish, A. J. Murchison, and J. B. Goodenough, Energy Environ. Sci. **10**, 331 (2017).
[10] C. Sun, J. Liu, Y. Gong, D. P. Wilkinson, and J. Zhang, Nano Energy **33**, 363 (2017).

[11] Y. Kato, S. Hori, T. Saito, K. Suzuki, M. Hirayama, A. Mitsui, M. Yonemura, H. Iba, and R. Kanno, Nat. Energy **1**, 16030 (2016).
[12] J. Janek and W. G. Zeier, Nat. Energy **1**, 16141 (2016).
[13] J. W. Choi and D. Aurbach, Nat. Rev. Mater. **1**, 16013 (2016).
[14] V. Thangadurai, S. Narayanan, and D. Pinzaru, Chem. Soc. Rev. **43**, 4714 (2014).
[15] J. Y. Hwang, S. T. Myung, and Y. K. Sun, Chem. Soc. Rev. **46**, 3529 (2017).
[16] Y. Wang, W. D. Richards, S. P. Ong, L. J. Miara, J. C. Kim, Y. Mo, and G. Ceder, Nat. Mater. **14**, 1026 (2015).
[17] P. Vashishta, J. N. Mundy, and G. Shenoy, in *Fast on Transport in Solids-Electrode and Electrolytes Conference, Lake Geneva, WI, USA, 21–25 May* (Elsevier North-Holland, Inc, New York, 1979), p. 771.
[18] A. Kvist, A. Bengtzelius, and U. Trolle, Z. Naturforsch. A **23**, 2042 (1968).
[19] X. He, Y. Zhu, and Y. Mo, Nat. Commun. **8**, 15893 (2017).
[20] S. Hull, Rep. Prog. Phys. **67**, 1233 (2004).
[21] X. Wang, R. Xiao, H. Li, and L. Chen, Phys. Rev. Lett. **118**, 195901 (2017).
[22] A. K. Sagotra, D. Chu, and C. Cazorla, Phys. Rev. Mater. **3**, 035405 (2019).
[23] B. Kozinsky, S. A. Akhade, P. Hirel, A. Hashibon, C. Elsässer, P. Mehta, A. Logeat, and U. Eisele, Phys. Rev. Lett. **116**, 055901 (2016).
[24] C. S. Cucinotta, G. Miceli, P. Raiteri, M. Krack, T. D. Kühne, M. Bernasconi, and M. Parrinello, Phys. Rev. Lett. **103**, 125901 (2009).
[25] M. K. Gupta, B. Singh, P. Goel, R. Mittal, S. Rols, and S. L. Chaplot, Phys. Rev. B **99**, 224304 (2019).
[26] M. K. Gupta, P. Goel, R. Mittal, N. Choudhury, and S. L. Chaplot, Phys. Rev. B **85**, 184304 (2012).
[27] J. Klarbring, N. V. Skorodumova, and S. I. Simak, Phys. Rev. B **97**, 104309 (2018).
[28] P. C. Aeberhard, S. R. Williams, D. J. Evans, K. Refson, and W. I. F. David, Phys. Rev. Lett. **108**, 095901 (2012).
[29] B. Singh, M. K. Gupta, R. Mittal, and S. L. Chaplot, J. Mater. Chem. A **6**, 5052 (2018).
[30] B. Singh *et al.*, Phys. Chem. Chem. Phys. **19**, 15512 (2017).
[31] M. H. Braga, A. J. Murchison, J. A. Ferreira, P. Singh, and J. B. Goodenough, Energy Environ. Sci. **9**, 948 (2016).
[32] W. D. Richards, Y. Wang, L. J. Miara, J. C. Kim, and G. Ceder, Energy Environ. Sci. **9**, 3272 (2016).
[33] R.-c. Xu, X.-h. Xia, S.-h. Li, S.-z. Zhang, X.-l. Wang, and J.-p. Tu, J. Mater. Chem. A **5**, 6310 (2017).
[34] S. Wenzel, S. Randau, T. Leichtweiß, D. A. Weber, J. Sann, W. G. Zeier, and J. Janek, Chem. Mater. **28**, 2400 (2016).
[35] X. Han *et al.*, Nat. Mater. **16**, 572 (2016).
[36] J. Briant and G. Farrington, J. Electrochem. Soc. **128**, 1830 (1981).
[37] Z. Zhang, E. Ramos, F. Lalère, A. Assoud, K. Kaup, P. Hartman, and L. F. Nazar, Energy Environ. Sci. **11**, 87 (2018).
[38] S.-H. Bo, Y. Wang, and G. Ceder, J. Mater. Chem. A **4**, 9044 (2016).
[39] C. Yu, S. Ganapathy, N. J. J. de Klerk, E. R. H. van Eck, and M. Wagemaker, J. Mater. Chem. A **4**, 15095 (2016).
[40] I.-H. Chu, C. S. Kompella, H. Nguyen, Z. Zhu, S. Hy, Z. Deng, Y. S. Meng, and S. P. Ong, Sci. Rep. **6**, 33733 (2016).
[41] X. Lei, Y. Jee, and K. Huang, J. Mater. Chem. A **3**, 19920 (2015).
[42] A. Pant, Acta Crystallogr. Sec. B: Struct. Crystallogr. Cryst. Chem. **24**, 1077 (1968).
[43] V. Kahlenberg, S. Rakić, and C. Weidenthaler, Z. Kristallogr.-Cryst. Mater. **218**, 421 (2003).
[44] V. Kahlenberg, G. Dörsam, M. Wendschuh-Josties, and R. Fischer, J. Solid State Chem. **146**, 380 (1999).
[45] A. Pant and D. Cruickshank, Acta Crystallogr. Sec. B: Struct. Crystallogr. Cryst. Chem. **24**, 13 (1968).
[46] Y. Jee, P.-H. Chien, E. Villarreal, Y.-Y. Hu, and K. Huang, Solid State Ionics **296**, 63 (2016).
[47] X. Lei, J. Wang, and K. Huang, J. Electrochem. Soc. **163**, A1401 (2016).
[48] A. Sayeed, S. Mitra, A. Anil Kumar, R. Mukhopadhyay, S. Yashonath, and S. Chaplot, J. Phys. Chem. B **107**, 527 (2003).
[49] O. Russina, A. Triolo, Y. Aihara, M. T. Telling, and H. Grimm, Macromolecules **37**, 8653 (2004).
[50] P. Zhao *et al.*, Nat. Commun. **10**, 999 (2019).
[51] F. Demmel and S. Mukhopadhyay, J. Chem. Phys. **144**, 014503 (2016).
[52] K. Funke, Philos. Mag. A **64**, 1025 (1991).
[53] G. Lucazeau, J. Gavarri, and A. Dianoux, J. Phys. Chem. Solids **48**, 57 (1987).
[54] W. Howells, A. Barnes, and M. Hamilton, Phys. B: Condensed Matter **266**, 97 (1999).
[55] T. Willis, D. Porter, D. Voneshen, S. Uthayakumar, F. Demmel, M. Gutmann, M. Roger, K. Refson, and J. Goff, Sci. Rep. **8**, 3210 (2018).
[56] M. T. Telling, S. I. Campbell, D. Engberg, D. M. y Marero, and K. H. Andersen, Phys. Chem. Chem. Phys. **18**, 8243 (2016)..
[57] F. Demmel *et al.*, Eur. Phys. J. Web Conf. **83**, 03003 (2015).
[58] R. Mittal, B. Singh, S. L. Chaplot, and S. Mukhopadhyay, Na-Dynamics in Solid Ionic Conductors: 11Al2O3-Na2O and Na2Ti3O7, STFC ISIS Neutron and Muon Source (2019), https://doi.org/10.5286/ISIS.E.101136986.
[59] O. Arnold *et al.*, Nucl. Instrum. Methods Phys. Res., Sect. A **764**, 156 (2014).
[60] S. Mukhopadhyay, B. Hewer, S. Howells, and A. Markvardsen, Phys. B: Condens. Matter **563**, 41 (2019).
[61] R. Mittal, S. Chaplot, N. Choudhury, and C. Loong, J. Phys.: Condens. Matter **19**, 446202 (2007).
[62] P. P. Bose, R. Mittal, and S. L. Chaplot, Phys. Rev. B **79**, 174301 (2009).
[63] S. L. Chaplot (unpublished).
[64] G. J. Ackland, K. D'Mellow, S. Daraszewicz, D. Hepburn, M. Uhrin, and K. Stratford, Comput. Phys. Commun. **182**, 2587 (2011).
[65] G. Kresse and J. Furthmüller, Comput. Mater. Sci. **6**, 15 (1996).
[66] G. Kresse and D. Joubert, Phys. Rev. B **59**, 1758 (1999).
[67] A. Togo and I. Tanaka, Scr. Mater. **108**, 1 (2015).
[68] J. P. Perdew, K. Burke, and M. Ernzerhof, Phys. Rev. Lett. **78**, 1396 (1997).
[69] J. P. Perdew, K. Burke, and M. Ernzerhof, Phys. Rev. Lett. **77**, 3865 (1996).
[70] H. J. Monkhorst and J. D. Pack, Phys. Rev. B **13**, 5188 (1976).
[71] S. Nosé, J. Chem. Phys. **81**, 511 (1984).

[72] M. P. Allen and D. J. Tildesley, *Computer Simulation of Liquids* (Oxford University Press, Oxford, 2017).
[73] V. F. Sears, Neutron News **3**, 26 (1992).
[74] A. Vispa, D. Monserrat, G. J. Cuello, F. Fernandez-Alonso, S. Mukhopadhyay, F. Demmel, J. L. Tamarit, and L. C. Pardo, Phys. Chem. Chem. Phys. **19**, 20259 (2017).
[75] M. Bee, *Quasielastic Neutron Scattering* (IOP, Bristol, England, 1988).
[76] P. L. Hall and D. Ross, Mol. Phys. **42**, 673 (1981).
[77] C. T. Chudley and R. J. Elliott, Proc. Phys. Soc. **77**, 353 (1961).
[78] S. Mukhopadhyay, P. V. Sushko, A. M. Stoneham, and A. L. Shluger, Phys. Rev. B **70**, 195203 (2004).